ON THE ROLE OF THE SURFACE DIELECTRIC CONSTANT FOR ICEPHOBIC COATING APPLICATIONS

R. Menini[1], M. Farzaneh[1], Z. Ghalmi[1] and Y. Thibault[2]
[1]NSERC / Hydro-Quebec / UQAC Industrial Chair on Atmospheric Icing of Power Network Equipment (CIGELE) and Canada Research Chair on Atmospheric Icing Engineering of Power Networks (INGIVRE), www.cigele.ca
Université du Québec à Chicoutimi (UQAC), Chicoutimi, QC, Canada
[2]Dual-ADE, Sherbrooke, QC, Canada
E-mail: rmenini@uqac.ca

Excessive ice and wet snow accumulation may cause serious problems to the integrity of outdoor equipments and structures such as transmission lines, wind turbines, telecommunication towers, aircrafts, *etc*. A new passive method to overcome such problems was recently put forward: the deposition of icephobic coatings on exposed surfaces. Currently these coatings have few industrial applications, but they are environmentally friendly compared to de-icing fluids, and are cheaper than thermal and mechanical methods. Low dielectric constant or low surface energy materials exhibit low ice adhesion strengths, and polytetrafluoroethylene (PTFE or Teflon®) is actually one of the best materials to meet this criteria. In the present study, different anodization processes on aluminum that can be followed by a hydrophobic impregnation process such as PTFE deposition were studied. The main objective was to correlate the dielectric constant value of the coating with the shear ice adhesion strengths measured using a centrifugal technique. Coating morphology and hydrophobic properties were also measured and analyzed. The measurement of coating dielectric constants is not straightforward since dielectric Al oxide layers are usually divided into of two dense and porous layers, see Fig. 1. Therefore, complex impedance spectroscopy measurements followed by data fitting using appropriate electronic equivalent circuits (see Fig. 2) were performed. Theory and experimental results were successfully related, see Fig. 3. This study will be necessary to correlate ice adhesion force data with the permittivity of a given coating.

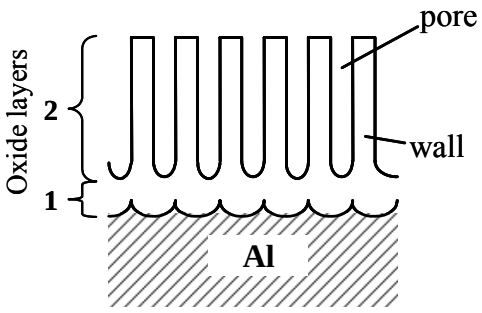

Figure 1. Schematic representation of the Al_2O_3 porous layer produced on Al 6061.

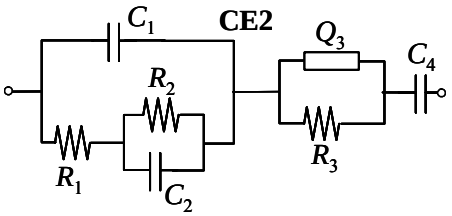

Figure 2. Equivalent electronic circuit CE2.

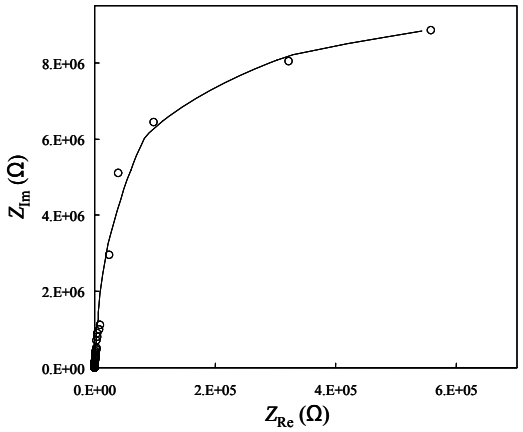

Figure 3. Experimental (○) and theoretical (CE2) (—) Nyquist plots for Al anodized sample at 60 minutes.

ON THE ROLE OF THE SURFACE DIELECTRIC CONSTANT FOR ICEPHOBIC COATING APPLICATIONS

R. Menini[1], M. Farzaneh[1], Z. Ghalmi[1] and Y. Thibault[2]
[1]*NSERC / Hydro-Quebec / UQAC Industrial Chair on Atmospheric Icing of Power Network Equipment (CIGELE) and Canada Research Chair on Atmospheric Icing Engineering of Power Networks (INGIVRE), www.cigele.ca*
Université du Québec à Chicoutimi (UQAC), Chicoutimi, QC, Canada
[2]*Dual-ADE, Sherbrooke, QC, Canada*
E-mail: rmenini@uqac.ca

Abstract
Excessive ice and wet snow accumulation may cause serious problems to the integrity of outdoor equipments and structures such as transmission lines, wind turbines, telecommunication towers, aircrafts, *etc*. A new passive method to overcome such problems was recently put forward: the deposition of icephobic coatings on exposed surfaces. Currently these coatings have few industrial applications, but they are environmentally friendly compared to de-icing fluids, and are cheaper than thermal or mechanical methods. Low dielectric constant or low surface energy materials exhibit low ice adhesion strengths and polytetrafluoroethylene (PTFE or Teflon®) is actually one of the best materials to meet this criteria.

In the present study, different anodization processes on aluminum that can be followed by a hydrophobic impregnation process such as PTFE deposition were studied. The main objective was to correlate the dielectric constant value of the coatings with ice adhesion shear strength (measured using a centrifugal technique). Coating morphology and hydrophobic properties were also measured and analyzed. The measurement of the coating dielectric constant is not straightforward since the dielectric Al oxide layers are usually divided into of two dense and porous layers. Therefore, complex impedance spectroscopy measurements followed by data fitting using appropriate electronic equivalent circuits were performed. Theory and experimental results were successfully related. This work will be very valuable to correlate ice adhesion force data with the permittivity of a given coating.

Keywords: Ice adhesion, anodization, porosity, permittivity, capacity, oxide layer, impedance spectroscopy.

I. INTRODUCTION

Recently, some studies have been focused on the development and application of icephobic coatings such as superhydrophobic materials to reduce ice adhesion force on exposed equipments during ice storms [1-5]. In order to engineer highly efficient coatings against ice adhesion, deep knowledge of the formation and the interaction of ice with a given material are needed.

The spraying of supercooled water droplets on a given surface and the resulting ice adhesion involve many parameters that can be divided into three groups: i) Forces involved at the ice-material interface; ii) Influence of the material surface roughness and iii) Influence of the icing conditions: T (^{o}C), wind speed, water droplet size, etc. Concerning surface roughness, its effect on ice adhesion strength is dictated by the chemical composition of the materials. For instance, micro- or nano rough surfaces of low surface energy materials may have very low ice adhesion strength such as in the case of superhydrophobic coatings [4]. On the other hand, rough high surface energy materials such as metals and oxides lead to strong ice shear stresses because of the mechanical anchoring effect [6]. Low temperatures and high wind speed usually lead to high adhesion strengths [7-8]. The current paper will focus on the first group of parameters, namely the forces involved at the ice-material interface. It is now well known that three intermolecular forces are involved during ice adhesion: electrostatic, hydrogen bonding and Van der Waals interactions [9]. It has also been demonstrated that the electrostatic component was by far the most important force compared to the other two [9]. In fact, electrostatic interactions occur between adhesives and substrates when they have different electronic band structures and both materials gain charge through an in-balance of charges. Electrostatic attraction theory is based on Coulomb's law and acceptor-donor interactions. Petrenko and Ryzhkin [9] theoretically studied in depth the electrostatic interaction taking place at ice/metal or ice/dielectric materials. Their theory is based on the Jacard theory that stated that electrical charge in ice is transferred by protonic point defects: **L**, **D**, H_3O^+ and OH^- which play a role similar to electrons and holes in electronic semiconductors. The empty bond is an **L**-defect and the bond with two protons

is a **D**-defect (doubly occupied). The other two defects correspond to ionic defects resulting from the water ionization reaction. At the ice crystal surface some of the protonic defects may be captured in the surface states, which have energies lower than those in the bulk of the ice. The capture of charged protonic defects in the surface states will result in a surface charge buildup, and therefore to the creation of a surface electric field. A charge q_{ice} on the ice surface induces an "image charge" at substrate material, q_{diel} in the case of polymers or oxides see Equation (1). In most solid dielectrics, ε_{diel} is much bigger than 1 and the induced charges are comparable with ones induced in metals. Lower is ε, lower is the electrostatic-related adhesion. For instance, Teflon® has a very low ε (2.04) and exhibits ice-phobic properties.

$$q_{diel} = q_{ice}\left(\frac{\varepsilon_{diel}-1}{\varepsilon_{diel}+1}\right) \qquad (1)$$

Thus, it is of primary importance to study the electrostatic interaction and particularly the influence of material permittivity on the ice shear stress. The present paper is based on the determination of the anodized aluminium oxide layer permittivity. Because of the porous nature of this layer, complex impedance spectroscopic fitting investigations have been performed. They showed excellent correlation between the experimental measurements and the simulation studies.

II. EXPERIMENTAL SETUP

A. Anodization

6061 aluminum alloy coupons (3 x 5 cm) were used to prepare all the coatings. Samples were partially polished. Prior to the anodization process the coupons were degreased using acetone, and then rinsed carefully with de-ionized water. Phosphoric acid solutions were prepared using de-ionized water. The counter electrode was a 5.08 x 7.62 cm 6061 Al alloy plate and the electrochemical reaction was carried out at constant voltage of 50 V at 18 ^{o}C. The only variable parameter was the electrolysis time. The oxide layers were observed by scanning electron microscopy.

B. Impedance measurements and simulation

The samples, alloy and their oxide layers were placed between two copper electrodes. The impedance analyzer Agilent 4294A was used to record complex data (Z_{Re} and Z_{Im}) at each frequency beginning at 2 MHz and finishing at 40 Hz. Curved fitting was performed using the Ramdomize-Simplex method of the EC-Lab® software from the Bio-Logic Company. Experimental Nyquist plots results (Z_{Re} vs Z_{Im}) have been compared to theoretically equivalent electronic circuits by minimizing the statistical parameter χ^2 for each fitting experiment, see equation (2).

$$\chi^2 = \sum_{i=1}^{n} \frac{\left[Z_{\exp}(i) - Z_{\mathrm{mod}}(f_i, par.)\right]^2}{\sigma_i^2} \qquad (2)$$

In this equation, Z_{exp} is the measured impedance at the f_i frequency, Z_{mod} is the impedance calculated using the chosen model at frequency f_i with the parameters of the equivalent electronic circuit (R, C, Q, L, etc.) and σ_i is the standard deviation.

III. RESULTS AND DISCUSSION

A. Anodized Al 6160 samples

Three different Al 6061 anodized samples were produced at three different electrolysis time: 32, 60 and 90 minutes. The corresponding micro-/nano- structures are shown in Fig. 1. The porous structure of the Al_2O_3 layer was clearly visible. It was also observed that the longer the anodisation time is, the thinner are the pore walls. This porous structure is typical of anodized samples and is schematically depicted in Fig. 2 where the oxide layer is composed of a dense layer adjacent to the metal and an outer porous layer. In order to evaluate the dielectric constant, the presence of air within the porous structure had to be taken in account. Knowing the dielectric constants of both air (ε = 1) and Al_2O_3 (ε = 10) [10] and by averaging the number and the pore surface of for a given area, see Fig. 1, an estimation of the theoretically effective dielectric constants of the three oxide layers is possible according to Equation (3). All the estimations are displayed in Table I.

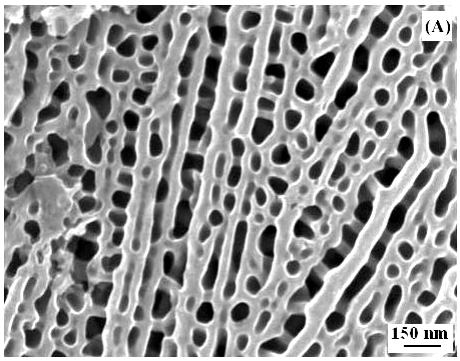

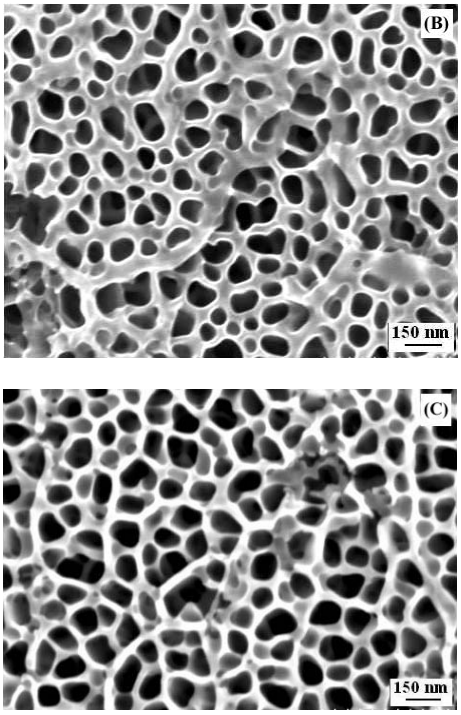

Figure 1. Anodized aluminum surface microphotographs: (A) 32, (B) 60 and (C) 90 minutes.

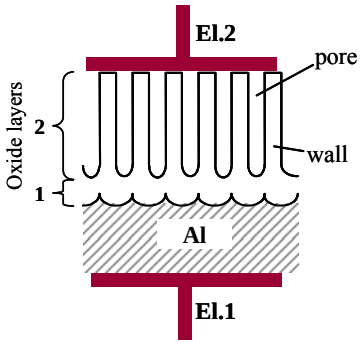

Figure 2. Schematic representation of the Al_2O_3 porous layer produced on Al 6061. The two copper electrodes (El.1 and El.2) are used for impedance measurements.

$$\varepsilon_{eff}\ theo. = \varepsilon_{air}\left(\frac{S_{air}}{S}\right) + \varepsilon_{Al}\left(\frac{S_{ox.}}{S}\right) \qquad (3)$$

The experimental dielectric constants were measured using the capacitance measured with the Agilent apparatus as well as the coating's thickness. It must be pointed out there that the ε_{eff} measurements were performed using a simple plane capacitor configuration. The corresponding data are shown in Table I. The discrepancies between the theoretical and experimental values can be explained by the fact that the Al_2O_3 layer structure is porous and that electrode El.2, see Fig. 2, is only in contact with the wall extremities of the outer oxide layer. Therefore, the assumption of plane capacitor is no longer valid.

TABLE I. Evaluation of theoretical dielectric constants

Anodization (min)	32	60	90
Pore dia. (nm)	70	90	140
S_{air} (nm^2)	$2.7\ 10^4$	$8.3\ 10^4$	$12.4\ 10^4$
$S_{ox.}$ (nm^2)	$13.3\ 10^4$	$7.3\ 10^4$	$3.6\ 10^4$
ε_{eff} theo.	8.48	5.33	3.07
ε_{eff} exp	0.38	0.50	0.34

To extract the proper ε_{eff} values from the complex data obtained with the Agilent apparatus, complex curve fitting have been performed using different equivalent circuits. Some researchers [11-12] studied the aluminium and titanium porous oxide layer using electrochemical impedance spectroscopy. The best fittings were observed using the equivalent electronic circuit CE1, see Fig. 3. For CE1, C_1 and R_1 represent the capacity and the resistance of the outer porous oxide layer, whereas C_2 and R_2 are related to the inner dense oxide layer. Finally Q_3 and R_3 are related to the porosity of the Al_2O_3 layer. Q_3 is a constant phase element that can be considered as a capacitance [11]. In the present research and using CE1 with the Ramdomize-Simplex method of the EC-Lab® software poor fittings were observed for the three anodized samples. It must be mentioned that the use of CE1 originated from electrochemical experiments and that the electrode El.2, shown in Fig. 2, is not present in such a wet system. Therefore another appropriate equivalent circuit had to be chosen. By adding a new capacitance C_4 in series with the circuit CE1 to obtained CE2 (Fig. 3), excellent fittings between the experimental and fitting curves were obtained for the three anodized samples (Fig. 4). In fact, the capacitance C_4 corresponds to the capacitance created at the El.2-porous oxide layer interface.

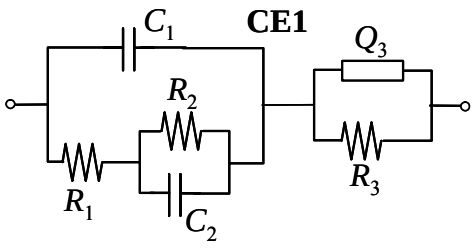

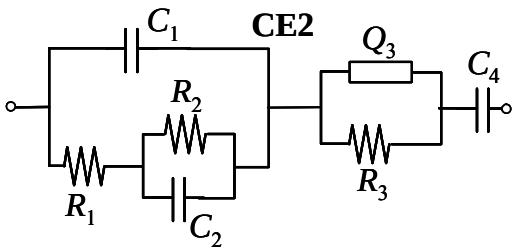

Figure 3. Equivalent electronic circuits CE1 and CE2.

Considering that $Q_3 = C_3$ and that C_4 is not representing a capacity intrinsic to the anodized layer, one can assume that the total capacity of the aluminum oxides layer can be calculated using Equation (4). The effective permittivity (ε_{eff} fit.) is calculated using Equation (5) while the data is obtained from curve fitting C_1 to C_3, see Table II. Considering that the surface area of electrode 2 (El.2) is $A = 1.77\ 10^{-4}$ m^2 and that the free space permittivity is $\varepsilon_0 = 8.85419\ 10^{-12}$ $C^2N^{-1}m^{-2}$, the computation results are displayed in Table II. It is clear that the effective permittivity values obtained through complex curve fitting are in the same range of the non-porous Al_2O_3 permittivity and are closer to the theoretical permittivities indicated in Table I. The results are compared in Fig. 5 showing coating thickness and permittivity plots against anodisation time. As expected for both ε_{eff} theoretical and ε_{eff} fitted values, the thicker is the coating the lower is the permittivity since thick Al_2O_3 coatings are more porous. For each anodization time, ε_{eff} theoretical < ε_{eff} fitted which can be explained by the fact that in calculating the theoretical value of ε_{eff} only the porous model was considered (see layer 2 in Fig. 2). The inner dense oxide layer 1 was not taken into account since it was very difficult to evaluate its thickness on the cross-sections of the metallographic samples. Nevertheless, complex impedance spectroscopy data fitting proved to be an excellent tool to assess the permittivity of anodized porous aluminum oxide.

$$C_{tot} = \frac{C_3\left(C_1 + C_2\right)}{C_1 + C_2 + C_3} \tag{4}$$

$$\varepsilon_{eff}\ fit = \frac{C_{tot}\, d}{\varepsilon_0\, A} \tag{5}$$

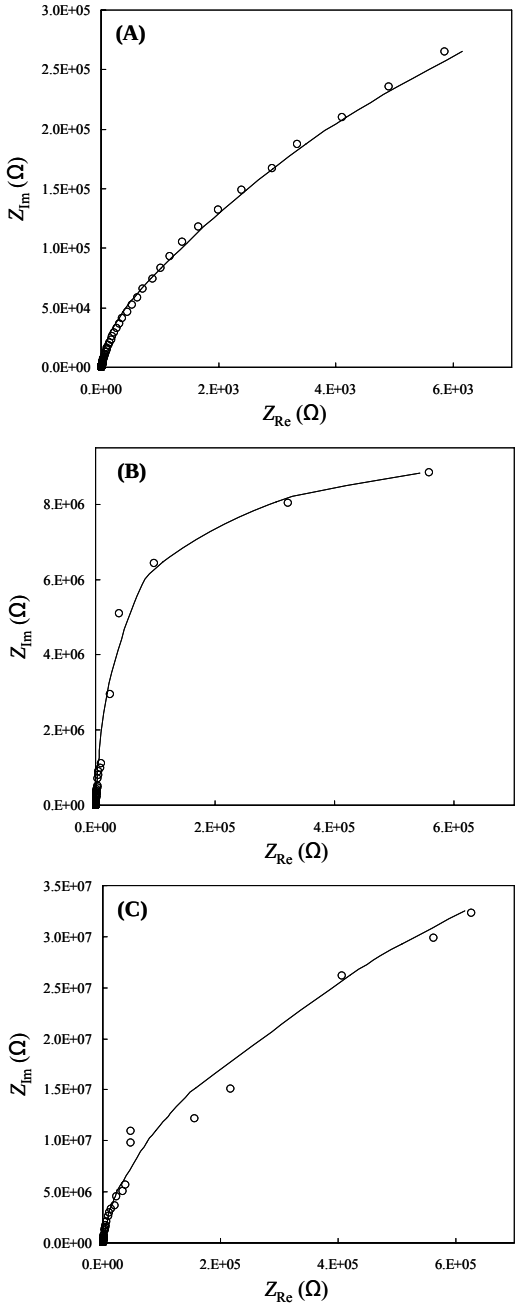

Figure 4. Experimental (○) and theoretical (CE2) (—) Nyquist plots for different anodized samples. (A) 32, (B) 60 and (C) 90 minutes.

TABLE II. ε_{eff} fit. values and complex curve fitting data (CE2).

Anod. (min)	32	60	90
C_1 (nF)	11.74	25.78	0.11
C_2 (nF)	8.18	7.08	1.88
C_3 (nF)	28.88	9.31	8.86
d (μm)	1.35	2	5

ε_{eff} fit.	10.16	9.26	5.19

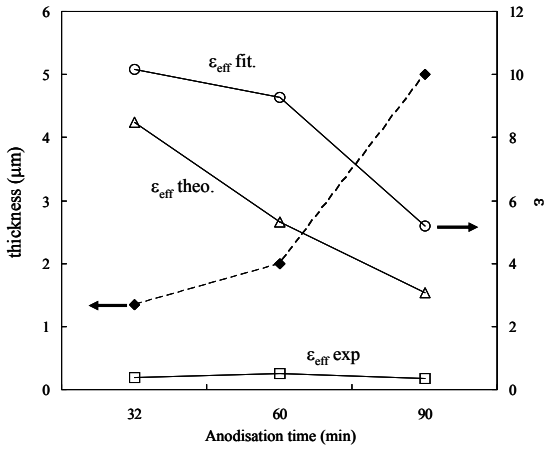

Figure 5. thickness and permittivity vs anodisation time.

IV. CONCLUSION

In order to correlate the dielectric constant of a given coating with the ice adhesion strength, it is very important to measure this constant with the best precision possible. If the coating is porous or chemically heterogeneous, simple impedance measurements were shown to be inaccurate. However, complex impedance spectroscopy data fitting revealed to be an excellent tool to assess the permittivity of porous aluminum oxide layers. Ice adhesion force measurements will be performed in further studies to validate the correlation between coating permittivity and ice shear stress. Other materials such as titanium oxides and different oxides impregnated with Teflon® will be also investigated.

ACKNOWLEDGMENTS

This work was carried out within the framework of the NSERC/Hydro-Quebec/UQAC Industrial Chair on Atmospheric Icing of Power Network Equipment (CIGELE) and the Canada Research Chair on Engineering of Power Network Atmospheric Icing (INGIVRE) at Université du Québec à Chicoutimi. The authors would like to thank the CIGELE partners Hydro-Québec, Hydro One, Réseau de Transport d'Électricité (RTE) and Électricité de France (EDF), Alcan Cable, K-Line Insulators, Tyco Electronics, Dual-ADE, and FUQAC) whose financial support made this research possible. The authors are grateful to Hélène Grégoire (National Research Council Canada, CTA, Chicoutimi, QC) for her technical assistance.

REFERENCES

[1] M. Farzaneh (Convenor), « Systems for prediction and monitoring of ice shedding, anti-icing and de-icing for overhead lines ». CIGRÉ WG B2.29, CIGRE Publications, Technical Brochure, Dec. 2010.

[2] A. Safaee, D.K. Sarkar and M. Farzaneh, «Superhydrophobic Properties of Silver-Coated Films on Copper Surface by Galvanic Exchange Reaction», Applied Surface Science, vol. 254, pp. 2493-2498, February 2008.

[3] D. Sarkar, M. Farzaneh and R. Paynter, «Superhydrophobic properties of ultrahin rf-sputtered Teflon films coated etched aluminium surfaces», Materials Letters, vol. 62, Issues 8-9, pp. 1226-1229, March 2008.

[4] N. Saleema, M. Farzaneh, R.W. Paynter and D.K.Sarkar, « Prevention of ice accretion on aluminium surfaces by enhancing their hydrophobic properties ». Journal of adhesion science and technology, vol.25, issue 1-3, janvier 2011, pp. 27-40

[5] R. Menini, Z.Ghalmi and M. Farzaneh, « Highly resistant icephobic coatings on aluminum alloys ». Cold Regions Science and Technology, vol.65, no.1, janvier 2011, pp.65-69.

[6] Z.Ghalmi, R. Menini and M. Farzaneh "Experimental study of the influence of the type of material, roughness and temperature on ice adhesion", IWAIS 2011, Chongqing, China, May 2011

[7] M. Kermani Kooshel, « Ice shedding from cables and conductors: a cracking model of atmospheric ice», PhD. Thesis, Université de Québec à Chicoutimi, 2007.

[8] J. Druez, C.L. Phan, J.L. Laforte and D.D. Nguyen, «Adhesion of glaze and rime on aluminum electrical conductors», Transaction of the Canadian society for mechanical engineering, vol. 5, pp. 215-220, 1978.

[9] I.A. Ryzhkin and V.F. Petrenko, « Physical Mechanisms Responsible for Ice Adhesion», J. Phys. Chem. B, Vol (101), pp 6267-6270, 1997.

[10] J. Robertson, « Band offsets of high dielectric constant gate oxides on silicon », Journal of non-crystalline Solids, 303, pp 94-100, 2002.

[11] R. Menini, M.J. Dion, S.K. Vicky So, M. Gauthier and L.P. Lefebvre, «Surface and Corrosion Electrochemical Caharacterization of Titanium Foams for Implant Application», Journal of the Electrochemical Society, V(153)-2006.

[12] Y. Huang, H. Shih, H. Huang, J. Daugherty, S. Wu, S. Ramanathan, C. Chang and F. Mansfeld, «Evaluation of the corrosion resistance of anodized aluminum 6061 using electrochemical impedance spectroscopy (EIS) », Corrosion Science, V(50), pp-3569-3575-2008.